Atmospheric Research 336 (2026) 108898

Contents lists available at ScienceDirect

Atmospheric Research

journal homepage: www.elsevier.com/locate/atmosres

Interannual co-variability of Tibetan Plateau Quasi-Biweekly oscillation intensity and asymmetric summer precipitation in China

Zhu Zhu [a,d], Meirong Wang [a,*], Jun Wang [b], Anmin Duan [c], Shunwu Zhou [a], Zhongshui Yu [e]

[a] State Key Laboratory of Climate System Prediction and Risk Management, Key Laboratory of Meteorological Disaster, Ministry of Education, Collaborative Innovation Center on Forecast and Evaluation of Meteorological Disasters, Nanjing University of Information Science and Technology, Nanjing, China
[b] International Institute for Earth System Science, Nanjing University, Nanjing, China
[c] State Key Laboratory of Marine Environmental Science, College of Ocean and Earth Sciences, Xiamen University, Xiamen, China
[d] College of Meteorology and Oceanography, National University of Defense Technology, Changsha 410073, China
[e] Mêdog Field Station for Scientific Observation and Research on Atmospheric Water Cycle/Xigazê and Mêdog National Climate Observatory, Tibet Meteorological Service, Lhasa, China

ARTICLE INFO

Keywords:
Tibetan Plateau
Quasi-Biweekly Oscillation Intensity
Interannual variability
Summer precipitation
Asymmetric connection

ABSTRACT

This study investigates the interannual variability in the intensity of the quasi-biweekly oscillation (QBWOI) of the atmospheric heat source over the Tibetan Plateau (TP) and its linkage with summer precipitation anomalies in China. The results reveal distinct propagation characteristics of quasi-biweekly signals between strong and weak QBWOI years. During strong QBWOI years, most quasi-biweekly oscillations propagate northward from low latitudes toward the TP, accompanied by enhanced moisture transport that converges over the southern TP. In contrast, during weak QBWOI years, outward propagation from the TP becomes more frequent, leading to regional moisture export. Corresponding to interannual variability in TP QBWOI, precipitation across China exhibits an asymmetric pattern: strong QBWOI years feature increased precipitation south of the middle and lower reaches of the Yangtze River, whereas weak years correspond to suppressed precipitation anomalies over the southern TP. The associated large-scale circulation patterns indicate that an East Asia-Pacific-like wave train contributes to the anticyclonic anomaly in the tropical Northwest Pacific during strong years, while two southeastward wave trains from Northern Europe and the Arctic in the mid-high latitudes, driven by the Arctic Oscillation, plays a more important role in forming a barotropic positive height anomaly over the northeastern TP in weak years. Overall, the TP QBWOI reflects systematic atmospheric configurations that are closely linked to interannual summer precipitation variability across China.

1. Introduction

Intraseasonal oscillations (ISOs) are a prominent feature of atmospheric variability not only in the tropics (Madden and Julian, 1971, 1972), but also in the mid- and high- latitudes (Jeong et al., 2008; Mao et al., 2010; Wen et al., 2011; Yang and Li, 2016). ISO-related large-scale circulations play a crucial role in shaping global weather and climate, influencing precipitation variability (Mao et al., 2010; Li and Mao, 2018), monsoon onset and evolution (Wang and Duan, 2015; Karmakar and Misra, 2019; Liu et al., 2024), and the occurrence of extreme events (Hsu et al., 2016; Zhang et al., 2021; Muhammad and Lubis, 2023).

Considerable attention has been paid to interannual variations in tropical ISOs, including oscillation periods, propagation characteristics, and intensity (Hendon et al., 1999; Kajikawa and Yasunari, 2005; Liu et al., 2016a; Wang and Chen, 2016; Wang and Wu, 2020; Wang et al., 2022a). Mechanistically, year-to-year changes in ISO intensity (ISOI) are governed by background atmospheric conditions in source regions, along propagation paths, and within affected zones (Kajikawa and Yasunari, 2005; Liu et al., 2016b; Wang and Wu, 2020). These interannual differences in tropical ISO characteristics can significantly influence tropical and extratropical weather systems, alter large-scale circulation, and shape multiscale climate anomalies (Diamond and Renwick, 2015; Li et al., 2019; Raghavendra et al., 2020). For instance, the establishment of low-level westerlies during the Indian summer monsoon onset and developing periods is strongly tied to ISOI (Qi et al., 2009). In the Western North Pacific, tropical cyclogenesis frequency shows greater sensitivity to ISOI of environmental factors than to seasonal mean anomalies or synoptic-scale variations (Cao et al., 2021).

* Corresponding author.
E-mail address: wmr@nuist.edu.cn (M. Wang).

https://doi.org/10.1016/j.atmosres.2026.108898
Received 10 September 2025; Received in revised form 11 February 2026; Accepted 27 February 2026
Available online 2 March 2026

Furthermore, tropical ISOI also modulates the structure and evolution of extratropical wave trains (Zheng and Chang, 2019), the Mei-yu onset (Yao et al., 2019), and the strength of upward motion over southern China (Zeng and Sun, 2023).

Tibetan Plateau (TP), acting as an active ISO center in the mid-latitudes, shows robust ISO signals in multiple meteorological elements, particularly in its summer atmospheric heat source (Yang and Li, 2017; Song et al., 2019; Zhong et al., 2020; Yuan et al., 2023). As an elevated heat source, the TP can directly heat the mid-troposphere and exert profound influence on regional and global weather and climate (Li et al., 2016; Han et al., 2024; Luo et al., 2024). Previous studies have demonstrated that the TP atmospheric heat source is dominated by quasi-biweekly oscillation (QBWO) signals (Zhu et al., 2018; Ren et al., 2019; Wang et al., 2019b; Zhu et al., 2025), with complex origins and diverse propagation pathways. These QBWO signals can propagate into the TP from low-latitude regions, driven by easterly vertical shear (Jiang et al., 2004) and moisture advection (Yang and Li, 2017), as well as mid- to high-latitudes associated with southeastward-propagating nonstationary wave trains (Wang and Duan, 2015; Yang and Li, 2017; Wang et al., 2018). Furthermore, the TP itself can serve as a source region, exporting ISO signals outward (Wang and Duan, 2015).

Notably, the ISO properties of the TP's atmospheric heat source also exhibit clear interannual variability. The primary oscillation period shows considerable year-to-year differences, most notably between 1978 and 1999 (Wang et al., 2009). The occurrence frequency and the propagation features of TP ISO also vary with years (Peng et al., 2012; Tian et al., 2023). Additionally, the interannual variations also exist in QBWO intensity (QBWOI) over the TP. For instance, Tian et al. (2023) addressed the impacts of TP QBWOI on intraseasonal precipitation in downstream areas. Zhu et al. (2025) further showed that TP ISOI is closely linked to a north-south reversal pattern in TP precipitation anomalies.

Compared to the extensive research on tropical ISOI variations and their climate impacts, considerably less attention has been given to the interannual variability of TP ISOI. In particular, the connections between TP ISOI and precipitation anomalies across China, as well as the underlying physical mechanisms, remain poorly understood. Given the dominance of QBWO signals in the TP region, this study aims to: (1) characterize the interannual variability of summer QBWOI in the TP atmospheric heat source, and (2) elucidate the relationship between this variability and precipitation anomalies over China, with a focus on the relevant dynamical and thermodynamical processes.

2. Data and methods

2.1. Datasets

This study employs daily atmospheric variables, including vertical velocity, horizontal wind, air temperature, and pressure from Japanese 55-year Reanalysis (JRA-55, Kobayashi et al., 2015), with a horizontal resolution of 1.25° × 1.25° and 12 vertical pressure levels (1000, 925, 850, 700, 600, 500, 400, 300, 250, 200, 150, and 100 hPa), to calculate the atmospheric apparent heat source. Additional variables such as divergence, vorticity, specific humidity, and sea-level pressure were also extracted from JRA-55 to support the analysis.

Monthly precipitation data are derived from the CN05.1 gridded dataset (Wu and Gao, 2013), which is based on interpolation from 2416 meteorological stations across China and has a spatial resolution of 0.25° × 0.25°. The monthly Arctic Oscillation (AO) index was obtained from the Climate Prediction Center of National Oceanic and Atmospheric Administration (NOAA CPC; https://www.cpc.ncep.noaa.gov/products/precip/CWlink/daily_ao_index/ao.shtml). The analysis focuses on the boreal summer season (June, July and August) during the period of 1979–2020.

2.2. Methods

The vertically integrated atmospheric apparent heat source, denoted as $< Q_1 >$, was calculated based on the residual budget method (Yanai, 1961; Yanai et al., 1973), as follows:

$$C_p\left[\frac{\partial T}{\partial t}+\vec{V}\bullet\nabla T+\left(\frac{p}{p_s}\right)^k\omega\frac{\partial\theta}{\partial p}\right]=Q_1, \tag{1}$$

$$< Q_1 >=\frac{1}{g}\int_{100}^{p_s} Q_1 dp, \tag{2}$$

where T, $\vec{V}$, p and p_s represent the air temperature, horizontal wind vector, atmospheric pressure, and surface pressure, respectively. The constant $k = R/C_p$, where R denotes the gas constant and C_p is the specific heat of dry air at the constant pressure. θ and ω are the potential temperature and vertical velocity. The reliability of the calculated $<Q_1>$ over the TP has been validated by Zhu et al. (2025) across multi-time scales using Atmospheric Heat Source Dataset based on satellite and routine meteorological observations (Duan et al., 2018), including long-term trends, interannual variability, and intraseasonal variations.

To isolate the QBWO signal of the atmospheric apparent heat source $<Q_1>$ over the TP, we first eliminated the climatological annual cycle (daily climatology and its first three harmonics) from the raw daily data. Subsequently, a Lanczos band-pass filter (Duchon, 1979) was used to extract the intraseasonal component within the quasi-biweekly band (typically 10–20 days). Then the summer-mean variance of the 10–20-day filtered $<Q_1>$ field for each year was defined as the TP QBWOI, representing the intensity of QBWO activity over the TP. To focus on interannual variability, a 2–7-year band-pass filter was applied to all variables prior to subsequent analyses.

To diagnose the propagation pathways of Rossby wave trains, the horizontal wave activity flux (WAF) was calculated following the formulation of Takaya and Nakamura (2001). The expression for horizontal WAF is as follows:

$$W=\frac{P\cos\varnothing}{2|U|}\begin{pmatrix}\frac{U}{a^2cos^2\varphi}\left[\left(\frac{\partial\psi'}{\partial\lambda}\right)^2-\psi'\frac{\partial^2\psi'}{\partial\lambda^2}\right]+\frac{V}{a^2cos^2\varphi}\left[\frac{\partial\psi'}{\partial\lambda}\frac{\partial\psi'}{\partial\varphi}-\psi'\frac{\partial^2\psi'}{\partial\lambda\partial\varphi}\right]\\ \frac{U}{a^2\cos\varphi}\left[\frac{\partial\psi'}{\partial\lambda}\frac{\partial\psi'}{\partial\varphi}-\psi'\frac{\partial^2\psi'}{\partial\lambda\partial\varphi}\right]+\frac{V}{a^2}\left[\left(\frac{\partial\psi'}{\partial\lambda}\right)^2-\psi'\frac{\partial^2\psi'}{\partial\varphi^2}\right]\end{pmatrix}, \tag{3}$$

where $|U| = (u, v)$indicates the horizontal flow, N^2 represents the buoyancy frequency squared, ψ' is the perturbation stream function, a is earth radius, P is the pressure/(1000 hPa). ϕ and λ denote the latitude and longitude, respectively.

In addition, prior to applying significance tests to filtered datasets, the effective degrees of freedom should be recalculated. This can be estimated using the method proposed by Bretherton et al. (1999), accounting for reduced temporal independence after filtering. For the objective classification of different QBWO propagation patterns, a k-means cluster analysis (Wang et al., 2019a) was conducted on the latitude–time diagrams of intraseasonal $<Q1>$ anomalies.

3. Propagation Characteristics Associated with TP QBWOI

The spatial distribution of 10–20-day filtered daily atmospheric heat sources ($<Q_1>$) over the TP during summer (1979–2020) exhibits a prominent north-south dipole pattern, with a robust center over the southern TP. This confirms previous findings that identify the region as a key center of QBWO activity (Yang and Li, 2017; Tian et al., 2023; Zhu et al., 2025) (Fig. 1a). Then the summer variance of the corresponding principal component (PC1) is calculated for each year and denoted as the raw QBWOI (Fig. 1b). To isolate its interannual variability, this raw

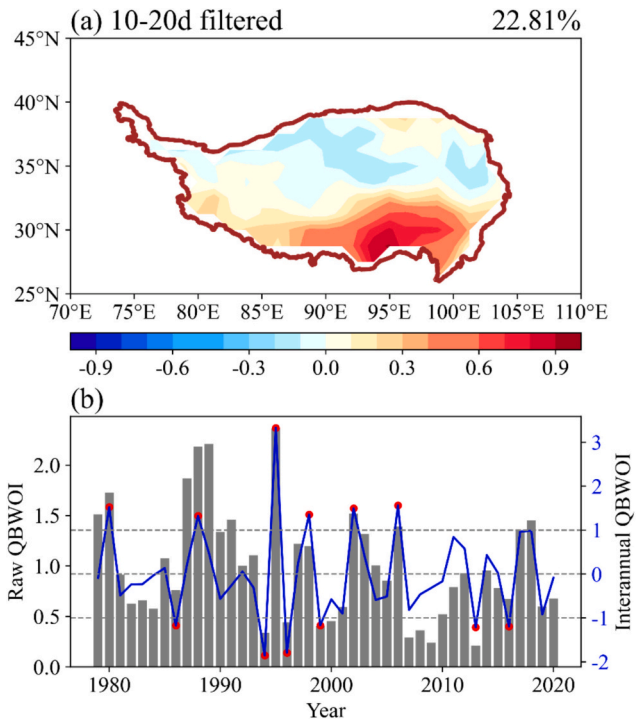

Fig. 1. The leading mode of QBWO in the TP summer $<Q_1>$ and its interannual variability. (a) The first EOF pattern of 10–20-day filtered summer $<Q_1>$ over the TP. (b) Raw time series (grey bars) and interannual variations (blue line) of the TP QBWOI during 1979–2020. Red dots mark years with strong ($> +1$ standard deviation) and weak (< -1 standard deviation) QBWOI. (For interpretation of the references to colour in this figure legend, the reader is referred to the web version of this article.)

QBWOI time series is then filtered using a 2–7-year bandpass filter, resulting in the interannual QBWOI used in subsequent analysis. Active (break) years are then identified as those in which the interannual QBWOI exceeds one standard deviation above (below) the mean. According to this criterion, 6 active years (1980, 1988, 1995, 1998, 2002, 2006) and 6 break years (1986, 1994, 1996, 1999, 2013, 2016) are selected from these 42-year record.

Variations in ISOI are closely linked to the propagation characteristics of ISO signals (Qi et al., 2019; Cheng et al., 2020; Wang et al., 2022b; Zeng and Sun, 2023). Focusing on the interannual timescale, we examine how QBWO propagation relates to the TP QBWOI. Based on the criterion requiring both trough and subsequent peak absolute values to exceed 0.75 standard deviations of PC1, 26 and 25 significant QBWO events are identified during strong and weak QBWOI years, respectively.

Meridional propagation of TP QBWO predominantly follows three pathways: (1) northward propagation from low latitudes into TP, (2) southward propagation from high latitudes into the TP, and (3) outward propagation from the TP toward higher and/or lower latitudes (Wang and Duan, 2015). Following Zhu et al. (2025), a QBWO event is classified as a significant northward propagation when it originates at or below 15°N and reaches the TP (25°N), showing clear northward propagation and temporal continuity, such as the cases around 15 and 25 August 1980 (Fig. 2). Similarly, an event is identified as significant southward propagation when it originates north of 50°N and propagates into the TP (south of 40°N), with evident southward propagation and temporal continuity (e.g., the events near 15 and 25 June 1980).

Based on the above classification criteria, the occurrence frequencies of different propagation types were identified and statistically analyzed (Table 1). Additionally, three strong and weak QBWOI years are selected as respective examples to demonstrate the contrasting latitude-time evolution of QBWO signals (Fig. 2). Clear differences in propagation characteristics are observed among years. During strong TP QBWOI years, 69% of significant QBWO events were accompanied by meridional propagation, with northward-propagating events dominating. In contrast, southward and outward propagations occurred less frequently (Fig. 2 and Table 1). During weak QBWOI years, 92% events involved meridional propagation. However, the frequency of northward-propagating events was markedly reduced, while southward propagation remained comparable to strong years. Notably, propagation outward from the TP emerged as the most prominent mode during weak QBWOI periods (Fig. 2 and Table 1). These results underscore distinct phase-dependent difference in QBWO propagation characteristics between strong and weak QBWOI years.

To further validate the above findings, a k-means cluster analysis was applied to the latitude-time diagrams of significant QBWO events. Based on the silhouette coefficient, the optimal number of clusters was determined to be two. Fig. 3 presents the composite results of these clusters. During strong QBWOI years (Fig. 3a and b), both clusters manifest pronounced northward propagation characteristics. Conversely, southward propagation fails to be distinguished as an independent cluster due to its relatively feeble QBWO signals, further underscoring the absolute dominance of northward propagation during active QBWOI periods. In contrast, weak QBWOI years reveal a markedly different regime: while Cluster1 maintains northward movements (Fig. 3c), the most prominent feature shifts to outward propagation from the TP toward both lower and higher latitudes (Fig. 3d), thereby diminishing the relative dominance of northward-moving disturbances. Specifically, 10 and 13 events fall into Cluster1 and Cluster2, respectively, during weak QBWOI years, indicating that outward propagation from the TP becomes the dominant mode during QBWOI break periods. These results are consistent with the manually identified propagation statistics shown in Table 1.

It is also noteworthy that northward-propagating events generally exhibit stronger QBWO signals than their southward counterparts (Figs. 2 and Fig. 3b). Therefore, even when the occurrence frequencies of northward and southward events are comparable, northward propagation continues to dominate (Table 1 and Fig. 3c and d).

The aforementioned analysis reveals a pronounced shift in the propagation characteristics of the QBWO signals from strong to weak QBWOI years. During strong QBWOI years, as illustrated in Fig. 3a and b, both clusters manifest distinct northward propagation patterns with obvious low-latitude anticyclonic anomalies driving substantial water vapor into the southern TP, resulting in the significant vapor convergence here (Fig. S1a and b). Furthermore, such a large-scale vibrant anticyclonic circulation also exists in the composite of all significant QBWO events during strong QBWOI years (Fig. S1c), as indicated by Wang and Duan (2015), which is the key circulation system in the QBWO northward propagations that can propel abundant vapor from low latitudes into the TP, suggesting that the critical influence of low latitudes in stimulating the TP QBWO activities during strong QBWOI years.

In summary, the northward-propagating QBWO from low latitudes is always stronger than its southward-propagating counterpart from high latitudes (Figs. 2 and 3). An increase in these northward events channels more moisture and stronger heat into the southern TP, where they converge and intensify the local QBWOI. Conversely, a decrease in such events allows outward propagation to dominate, dispersing QBWO signals from the TP to high and low latitudes, and thereby weakening the local QBWOI.

4. Asymmetric Linkages between TP QBWOI and China summer precipitation pattern

Given the profound climate effects of summer thermal forcing over the TP, particularly its close linkages with local and downstream precipitation anomalies (Wu et al., 2017; Han et al., 2024; Luo et al., 2025), this study systematically examines the potential interannual relationship between the TP QBWOI and summer precipitation anomalies across China. Composite results for summer precipitation during strong and

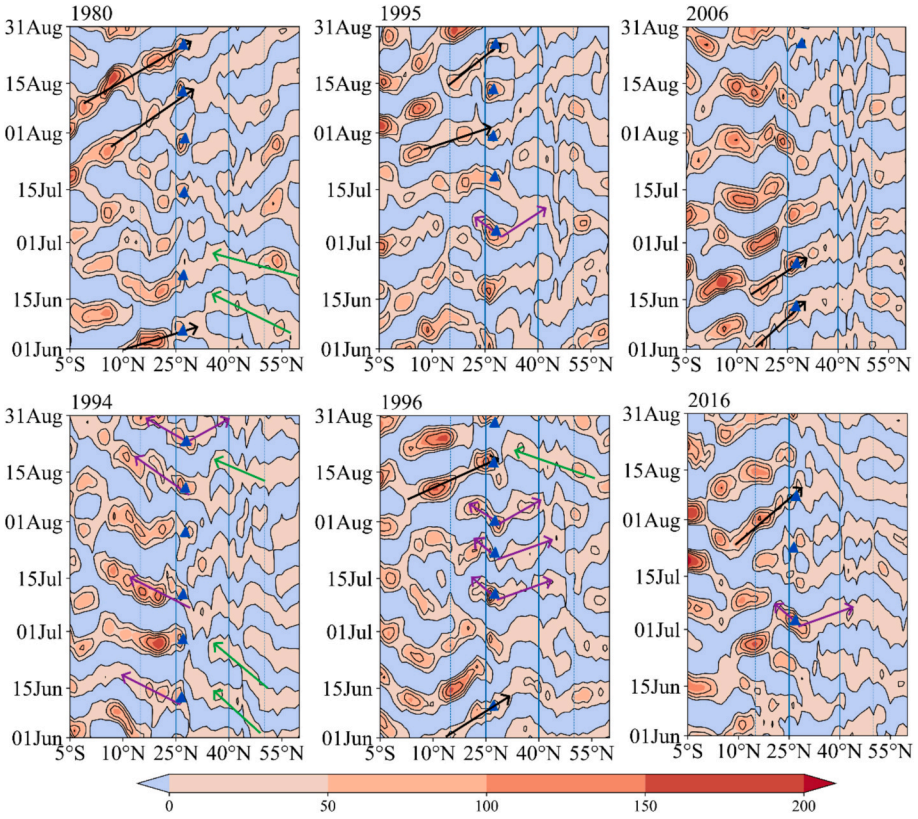

Fig. 2. Hovmöller diagrams of 10–20-day filtered $<Q_1>$ along 70° ~ 100°E for three representative cases during strong (top) and weak (bottom) QBWOI years. Blue triangles represent significant QBWO events. Black, green and purple arrows indicate significant northward propagation from low latitudes, southward propagation from high latitudes, and outward propagation from the TP to higher and/or lower latitudes, respectively. Thick vertical lines outline the longitudinal extent of the TP; thin vertical lines indicate 15°N and 50°N latitudes. (For interpretation of the references to colour in this figure legend, the reader is referred to the web version of this article.)

Table 1
Frequency of significant QBWO propagation events during strong and weak QBWOI years. Events are categorized as: Type I – northward propagation from low latitudes into the TP; Type II – southward propagation from high latitudes into the TP; and Type III – outward propagation from the TP toward high and/or low latitudes.s

QBWOI	Type I	Type II	Type III
Strong years	9	6	3
Weak years	6	6	11

weak QBWOI years are presented in Figs. 4a and b, along with their difference field (Fig. 4c). Clearly, precipitation anomalies exhibit distinctly asymmetric features between strong and weak QBWOI years. In strong years, a significant positive precipitation anomaly dominates the area south of the middle and lower Yangtze River (Fig. 4a). In contrast, weak QBWOI years feature a dipole anomaly, with an insignificant positive anomaly north of the lower Yangtze River and an insignificant negative anomaly to the south, accompanied by a pronounced negative anomaly over the southern TP (Fig. 4b). Given the relatively confined spatial extent of this dipole pattern and generally insignificant precipitation responses, the southern TP is identified as the key precipitation region for weak QBWOI years in subsequent analyses.

In summary, summer precipitation exhibits a clear QBWOI-phase-dependent anomaly: the strong TP QBWOI phase is accompanied by significantly enhanced rainfall south of the middle and lower Yangtze River, whereas the weak phase coincides with significantly reduced precipitation over the southern TP. These two key areas of precipitation anomalies are particularly evident in the precipitation difference field between strong and weak QBWOI years (Fig. 4c). Furthermore, the regression pattern of precipitation onto the TP QBWOI (Fig. S2) closely resemble the composite difference shown in Fig. 4c, further confirming the asymmetric associations of TP QBWOI with summer precipitation pattern across China.

The composite moisture flux and its divergence for strong and weak QBWOI yeas are presented in Figs.4d and 4e. In strong QBWOI years (Fig. 4d), a pronounced cyclonic–anticyclonic dipole anomaly in water vapor flux is evident over the northwestern Pacific. This feature consists of a cyclonic center located north of 30°N and a particularly robust anticyclonic center situated between 10°N–30°N, which enhances the southwesterly moisture transport. In contrast, weak QBWOI years (Fig. 4e) feature distinctly different circulation characteristics: the anticyclonic component weakens and shifts noticeably northward over the Yellow Sea. This allows the southern cyclone to intensify and extend westward over the Indian subcontinent and the Indo-China Peninsula, ultimately forming a new northeast-southwest-oriented dipole.

The distinct circulations between strong and weak QBWOI years establish correspondingly different moisture configurations, which ultimately shapes the asymmetric precipitation patterns across China. During strong QBWOI years, enhanced southerly flow forms a persistent moisture corridor extending from the tropical western Pacific to the middle and lower Yangtze River basin. The resulting strong moisture convergence provides favorable dynamic and thermodynamic conditions for enhanced precipitation (Fig. 4a and d). Conversely, during weak QBWOI years, widespread easterly wind anomalies along the southern flank of the TP boost moisture divergence over the region, leading to pronounced precipitation suppression (Fig. 4b and e). Such persistent easterly anomalies over the southern TP are a recognized precursor to drought conditions, as documented in previous studies (Wang et al., 2022b; Luo et al., 2023).

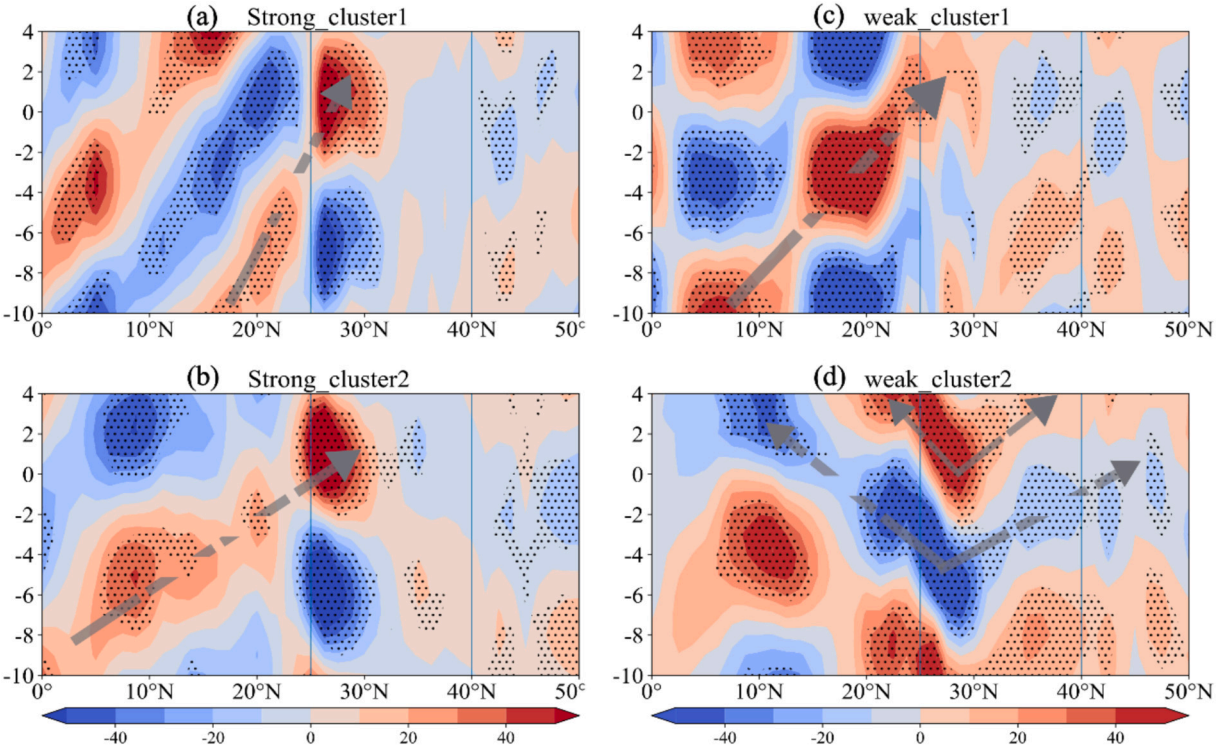

Fig. 3. Two leading clusters of latitude-time evolution of 10–20-day filtered $<Q_1>$ (W m^{-2}), averaged over 70° ~ 100°E, during (a, b) strong and (c, d) weak QBWOI years. Shaded areas with dots indicate regions exceeding the 90% confidence level. The two vertical lines represent the longitudinal extent of the TP. The '0' in Y-axis denotes the peak timing of the QBWO over the TP.

Actually, these circulation changes during strong and weak QBWOI years can also further modulate QBWO activity over the TP, thereby contributing to the interannual variability of QBWOI. This highlights the complex coupling among TP QBOWI, large-scale circulation, and precipitation. For instance, in the strong QBWOI years, the pronounced anomalous anticyclone over the northwestern Pacific facilitates the meandering transport of water vapor toward India and subsequently into the southern TP (Fig. 4d), which may help enhance the local QBWO activity. In contrast, in the weak QBWOI years, the strong cyclonic anomaly over India diverts water vapor away from the TP and blocks low-latitude moisture inflow (Fig. 4e), thereby potentially suppressing the northward-propagating QBWO.

5. The Associated Large-scale Circulation Patterns and Potential Mechanisms

Fig. 5 illustrates composite patterns of geopotential height and wind fields at both upper and lower levels during strong and weak TP QBWOI years. During strong QBWOI years, a distinctive "+ − +" geopotential height anomaly pattern emerges over the northwestern Pacific, forming a prominent barotropic structure evident at both upper and lower levels (Fig. 5a–c). Such a configuration enhances westerly flow to the east of the Yangtze River and establishes a marked westerly anomaly center over Japan in the upper troposphere (Fig. 5a). Importantly, the key region south of the middle and lower Yangtze River lies to the right of the entrance region of this upper-level jet anomaly (Fig. 5a), a location favorable for upper-level divergence (Fig. 5f). At mid-and lower levels, the anomalous anticyclone over the northwestern Pacific supports westward extension of the subtropical high, intensifying southerlies over southern China (Fig. 5b and c). The resulting convergence between these enhanced southerlies and northerly flow in the key region (Fig. 5c and f), facilitates significant upward motion (Fig. S3a), dynamically supporting the observed enhanced precipitation (Fig. 4a).

In contrast, during weak QBWOI years, the aforementioned "+ − +" anomalous geopotential height pattern over the northwestern Pacific vanishes. Instead, a robust positive geopotential height anomaly develops northeast of the TP, with a coherent barotropic structure evident in both upper and lower tropospheric levels (Fig. 5d and e). This anomaly shifts the upper-level westerly jet northward and generates persistent easterly flow over the TP (Fig. 5d). The resulting upper-level convergence over the southern TP, combined with lower-level divergence driven by the anomalous anticyclone northeast of the TP (Fig. 5d–5f), produces strong and extensive subsidence (Fig. S3b). This vertical circulation pattern suppresses convection and inhibits precipitation development over the southern TP, consistent with the negative precipitation anomalies observed during weak QBWOI years (Fig. 4b). Simultaneously, this broad subsidence will increase the atmospheric stability and weaken the local QBWOI. This indicates that the close relationship between weak TP QBWOI and precipitation anomalies is relatively limited and only significant in local areas of southern TP.

During strong QBWOI years, the anomalous geopotential height field over the northwestern Pacific exhibits a characteristic "+ − +" wave train pattern (Fig. 5a–c), consistent with the well-documented East Asia-Pacific (EAP) teleconnection pattern widely reported in previous studies. The upper-level anomalous anticyclone over the TP intensifies the South Asia High (Fig. 5a), the pronounced convergence along the southeastern flank of this TP anomalous anticyclone will induce intense sinking motions around Philippines region, facilitating the development and maintenance of the Northwest Pacific anomalous anticyclonic anomaly (Luo et al., 2023). This ultimately favors the excitation of a northward-propagating EAP-like wave train (Fig. 6). Previous studies (Yang et al., 2010; Zhu et al., 2023) have highlighted the critical role of the EAP teleconnection pattern as a conduit for enhanced moisture transport into the Yangtze River Basin, which helps support the substantial positive precipitation anomalies observed during strong QBWOI years (Fig. 4a).

During weak QBWOI years, the frequency of northward-propagating QBWO events decreases markedly, significantly weakening the

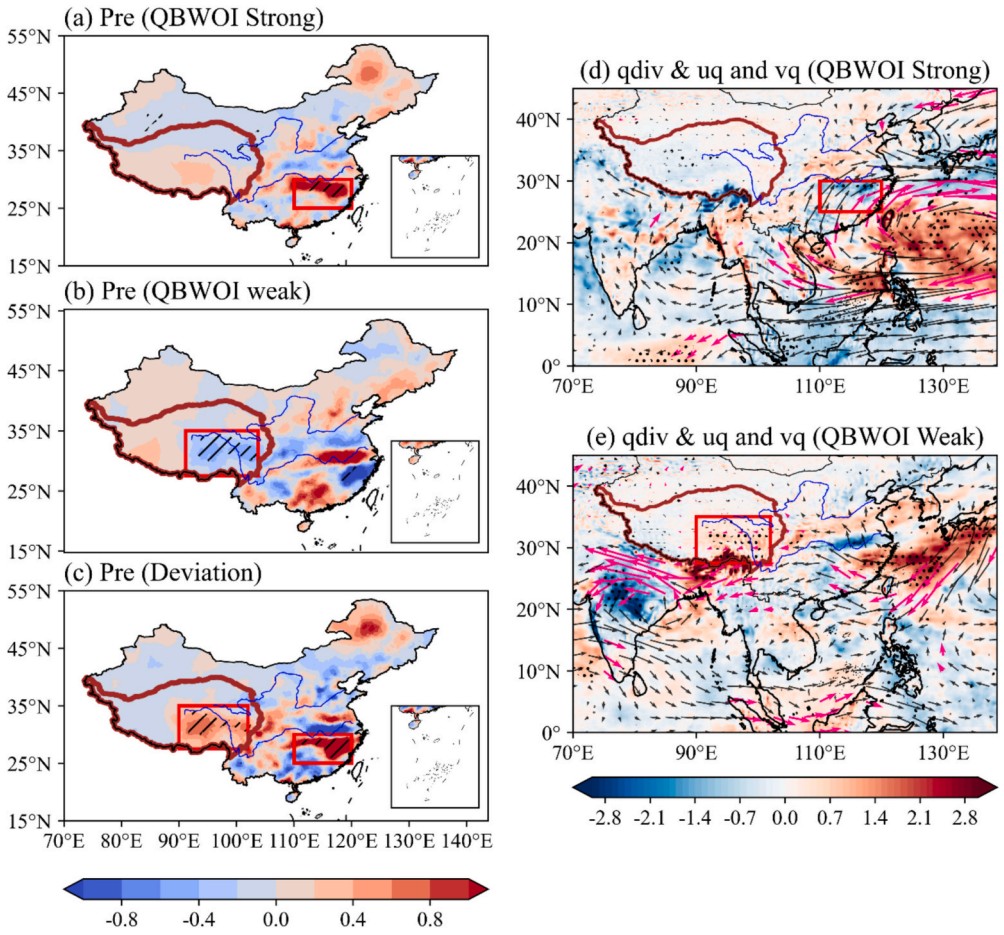

Fig. 4. Composite summer anomalies of (a and b) precipitation (mm/day), (d and e) the vertically integrated water vapor flux (vectors; kg m^{-1} s^{-2}), and moisture flux divergence (shaded, 10^{-5} kg m^{-2} s^{-2}) during (a and d) strong and (b and e) weak QBWOI years. (c) Differences in precipitation between strong and weak QBWOI years. Red boxes highlight the key precipitation regions closely linked to TP QBWOI. Pink vectors and dotted areas exceed the 90% confidence level. (For interpretation of the references to colour in this figure legend, the reader is referred to the web version of this article.)

regulatory influence of low-latitude systems on TP QBWO activity. This raises a key question: To what extent do mid- to high-latitude QBWO signals, as a secondary source, dominate TP QBWO variability under these suppressed conditions? Supporting evidence is provided by Wang et al. (2018), who showed that QBWO signals linked to the Arctic Oscillation (AO) can propagate southeastward toward the TP through a coherent barotropic wave train, thereby modulating the QBWO characteristics of the TP summer monsoon.

Composite patterns of sea level pressure (SLP) during strong and weak TP QBWOI years, along with the regression of SLP onto the summer AO index, are shown in Fig. 7. During weak TP QBWOI years, a prominent dipole pattern emerges in SLP, with a negative anomaly over the Arctic and a positive anomaly over subpolar regions (Fig. 7b). This spatial configuration closely mirrors the regression pattern associated with the AO index (Fig. 7c), suggesting that the AO may play a significant role in modulating TP QBWO variability during these periods. In contrast,

this dipole pattern is absent during strong TP QBWOI years (Fig. 7a), indicating a pronounced asymmetry in the AO-TP QBWOI relationship. The AO's influence on TP QBWO activity thus appears to be more prominent and statistically significant during weak QBWOI phases.

In addition, Fig. 7 illustrates the composite geopotential height and associated wave activity flux (WAF) in weak TP QBWOI years, along with the corresponding regression fields onto the AO index. As shown in Fig. 7d, two prominent southeastward-propagating wave trains emerge during weak TP QBWOI years: one originating from northern Europe and the other from the Arctic. These two wave trains converge over central Eurasia and subsequently extend toward the TP, ultimately resulting in a positive height anomaly over the northeastern TP. A comparable pattern is evident in the regression fields onto the AO index (Fig. 7e), indicating that the AO drives these wave trains under weak QBWOI conditions. Together, they contribute to the formation of the northeastern TP positive height anomaly, which suppresses precipitation over the southern TP. In addition, the AO-related wave trains in the mid-high latitudes appear to suppress the TP QBWOI through two primary pathways. First, they inhibit the northward advance of tropical airflows and fostering an anomalous cyclone over the Indian subcontinent, which reduces moisture transport to the TP (Fig. 4e); Second, they suppress local convection (Fig. S3b), thereby enhancing atmospheric stability and further weakening QBWOI.

In contrast, such mid-to-high latitude wave trains are absent during strong TP QBWOI years. Instead, the EAP wave train dominates, with its tropical anticyclonic anomaly acting as the key driver of enhanced precipitation south of the middle and lower Yangtze River (Fig. 4a and 6). In tandem, intensified southerly flows enhance moisture transport toward the TP, promoting the development of local QBWOI.

6. Summary and discussions

6.1. Summary

This study systematically examines the interannual variability characteristics of the TP QBWOI and its relationships with summer precipitation anomalies across China during the period 1979–2020.

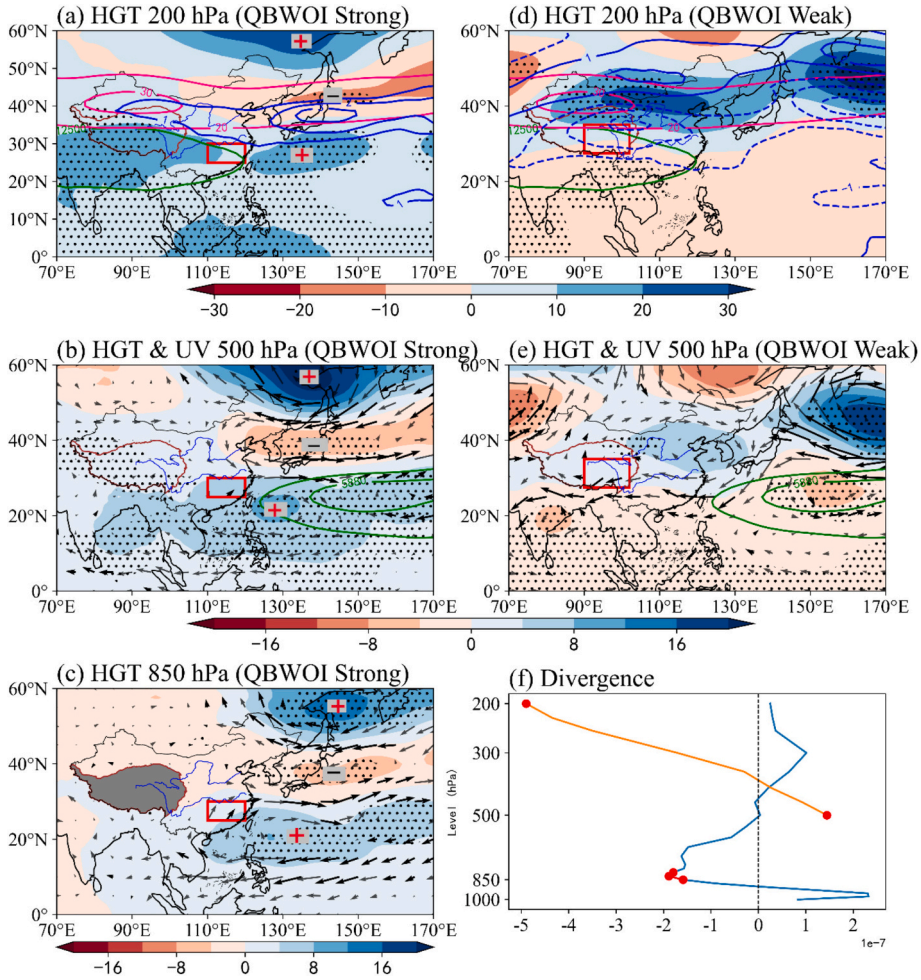

Fig. 5. Composite circulation patterns associated with strong and weak TP QBWOI years. (a, d) Geopotential height (shading; gpm) and zonal wind climatology (green contours), climatological zonal wind (pink contours) at 200 hPa during strong (left) and weak (right) QBWOI years, respectively. (b, e) Geopotential height (shading; gpm) and horizontal winds (vectors; m s^{-1}) at 500 hPa, with green contours indicating the 5880 and 5870 gpm climatological geopotential heights. (c) Same as (b) but for 850 hPa during strong QBWOI years. (f) Vertical profiles of divergence (s^{-1}) averaged over two key regions: the area south of the middle and lower Yangtze River (25°N–30°N, 110°E–120°E; blue line) during strong QBWOI years, and the southern TP (27.5°N–35°N, 90°E–102°E; orange line) during weak QBWOI years. Red dots in (f), bold vectors, and dotted regions in (a–e) denote areas statistically significant at the 90% confidence level. (For interpretation of the references to colour in this figure legend, the reader is referred to the web version of this article.)

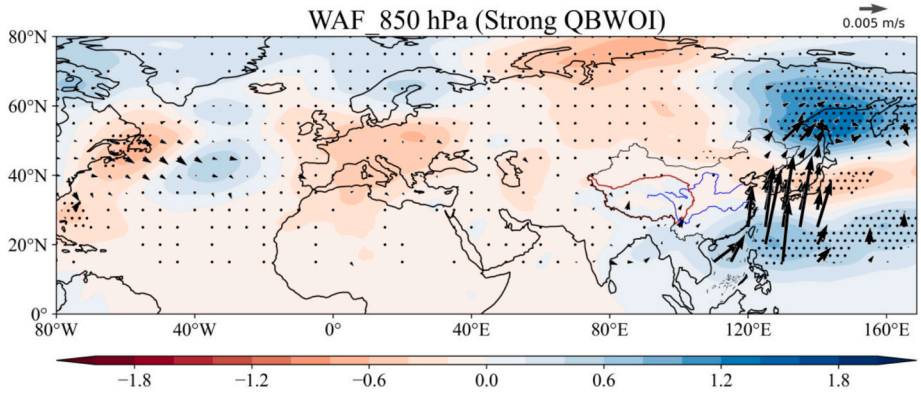

Fig. 6. Composite summer geopotential height anomalies (shaded, units: gpm) and associated wave activity flux vectors (units: $m^2 \cdot s^{-2}$) at 850 hPa during strong TP QBWOI years. Dotted areas indicate regions exceeding the 90% confidence level based on a two-tailed Student's *t*-test.

Notably, the interannual variability of the TP QBWOI is strongly modulated by the meridional propagation characteristics of QBWO signals, with markedly different dominant propagation patterns during strong and weak TP QBWOI years. In strong years, northward-propagating disturbances originating from low latitudes primarily contribute to QBWO activity over the TP. In contrast, during weak QBWOI years, the reduced frequency of such northward events diminishes the influence of low-latitude systems, shifting the dominant

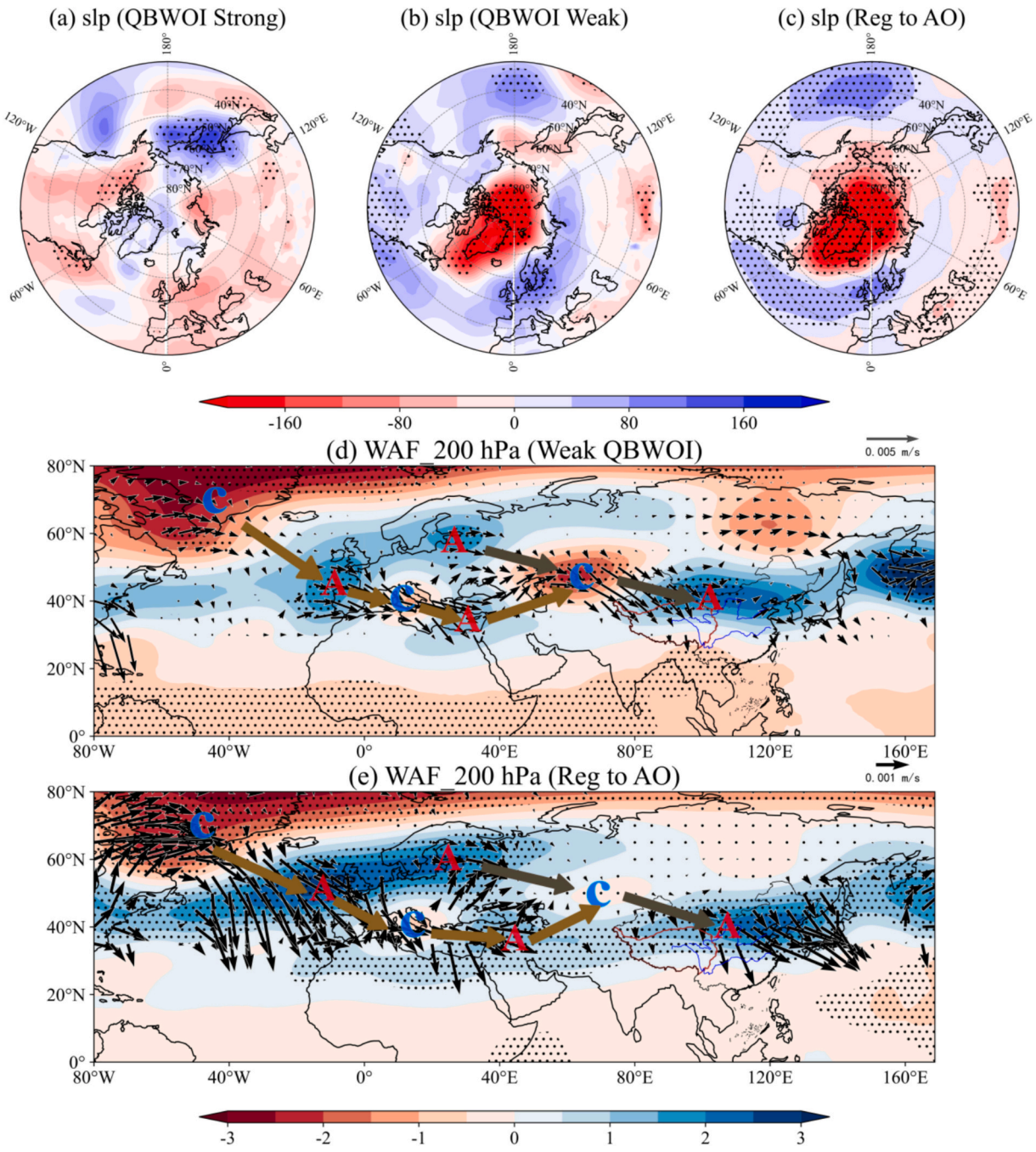

Fig. 7. Composite results during (a) strong and (b, d) weak TP QBWOI years, and (c, e) regression fields onto the summer Arctic Oscillation (AO) index, including: (a–c) Sea Level Pressure (SLP; Pa); (d–e) summer geopotential height (shaded, units: gpm) and wave activity flux (vectors, units: $m^2 \cdot s^{-2}$) at 200 hPa over the period of 1979–2020. Dotted areas indicate regions exceeding the 90% confidence level.

pattern toward energy dispersion from the TP to both lower and higher latitudes.

Furthermore, the TP QBWOI exhibits notable asymmetric linkages with summer mean precipitation over China. Strong TP QBWOI years are characterized by pronounced positive precipitation anomalies south of the middle and lower Yangtze River, whereas weak QBWOI years correspond to significant precipitation deficits over the southern TP. These contrasting precipitation patterns are associated with distinct large-scale circulation regimes. During strong TP QBWOI years, an EAP-like teleconnection emerges, characterized by a "+ − +" geopotential height anomaly pattern. Within this configuration, the tropical Northwest Pacific anticyclone plays a dual role: (1) facilitating enhanced moisture transport toward south of the Yangtze River, and (2) creating favorable dynamical conditions for ascent, both of which support increased precipitation in the region (Fig. 8a). In contrast, weak QBWOI years are marked by a mid-to-high latitude signal. Two AO-related wave trains, originating from Northern Europe and the Arctic, propagate southeastward, converge over central Eurasia, and extend toward the northeastern TP. These southeastward wave trains likely prohibit the northward extension of airflows from the tropics, leading to a strong cyclonic anomaly over the Indian subcontinent, blocking low-latitude moisture inflows and diverting moisture away from TP. Simultaneously, a barotropic height anomaly over the northeastern TP induced by these AO-related trains also provides the dynamic conditions for subside and associates with the suppressed precipitation over the southern TP (Fig. 8b).

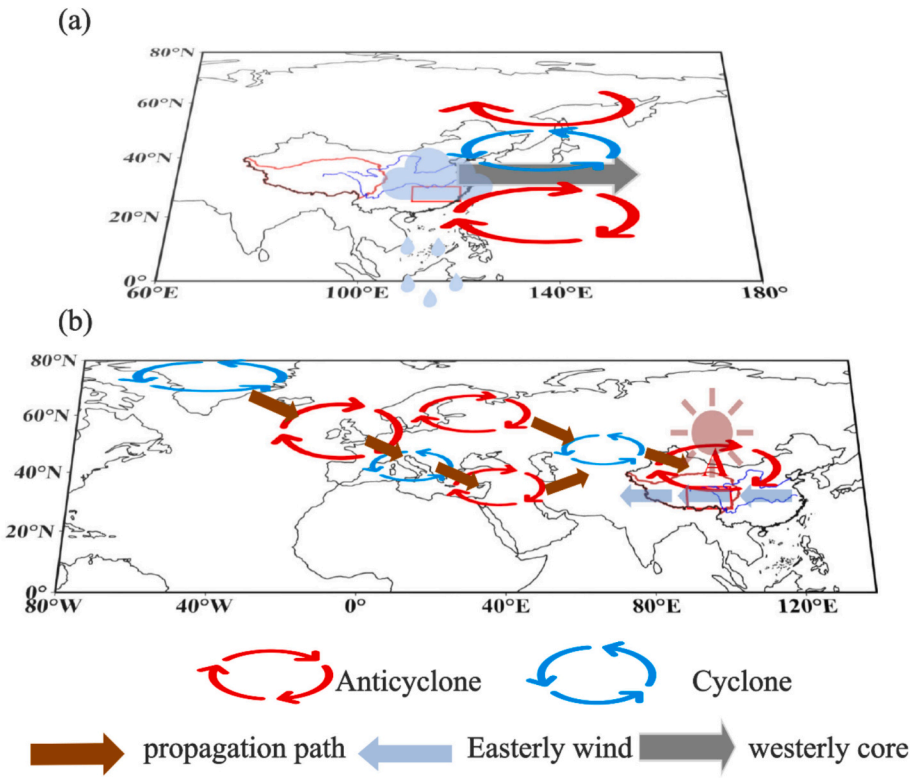

Fig. 8. Schematic illustration of the key circulation systems and associated physical processes linked to (a) positive precipitation anomalies south of the middle and lower Yangtze River during strong TP QBWOI years, and (b) negative precipitation anomalies over the southern TP during weak TP QBWOI years.

Together, these findings highlight a latitude-dependent regime shift in the large-scale circulation patterns linked to TP QBWOI variability: tropical systems are more closely associated with precipitation anomalies south of the middle and lower Yangtze River during strong QBWOI years, while mid-to-high latitude processes are more closely linked to precipitation deficits over the southern TP during weak years.

6.2. Discussion

Our results reveal an asymmetric relationship between TP QBWOI and summer precipitation anomaly; however, the causal direction remains uncertain. One possible interpretation is that TP QBWOI actively modulates large-scale circulation systems, which in turn influence precipitation. During strong QBWOI years, enhanced northward-propagating disturbances from low latitudes strengthen QBWO activity over the TP, while the accompanying EAP-like "+ − +" teleconnection pattern promotes moisture convergence and dynamical ascent south of the Yangtze River. Such intra-seasonal signals have been shown to influence East Asian monsoon, circulation adjustments, and regional rainfall variability (Fujinami and Yasunari, 2009; Li and Mao, 2018; Wang et al., 2019b; Tian et al., 2023**).** If this mechanism is valid, TP QBWOI could serve as an active intraseasonal precursor, providing a favorable tropical circulation background that regulates precipitation over China.

Alternatively, QBWOI and precipitation anomalies may both respond to the prevailing large-scale circulation rather than a direct causal forcing. QBWO propagation characteristics are strongly modulated by background circulation: strong TP QBWOI years coincide with circulation states that facilitate northward-propagating events, whereas weak years correspond to AO-related wave trains and barotropic height anomalies over the northeastern TP that suppress both moisture transport and QBWO activity. Precipitation anomalies align with these circulation regimes as well: the tropical Northwest Pacific anticyclone favors rainfall south of the Yangtze River in strong years, while AO-related disturbances reduce moisture availability over the southern TP during weak years. This suggests that TP QBWOI may act more as a dynamical indicator rather than a primary driver of circulation variability (Lu et al., 2023; Luo et al., 2023).

Overall, the observed TP QBWOI–precipitation relationship likely reflects a combination of direct intraseasonal forcing and shared responses to large-scale circulation patterns. Future studies should employ advanced statistical methods and numerical experiments to isolate the independent role of TP QBWOI, while also considering the influence of other climate modes such as ENSO and the Indian Ocean Dipole (Yang et al., 2022; Zhang et al., 2023; Kan et al., 2025). Such efforts would clarify the mechanisms linking TP intraseasonal variability with regional precipitation anomalies and improve subseasonal prediction.

CRediT authorship contribution statement

Zhu Zhu: Visualization, Methodology, Investigation, Data curation. **Meirong Wang:** Writing – review & editing, Supervision, Conceptualization. **Jun Wang:** Writing – review & editing. **Anmin Duan:** Writing – review & editing. **Shunwu Zhou:** Writing – review & editing. **Zhongshui Yu:** Writing – review & editing.

Declaration of competing interest

The authors declare that they have no known competing financial interests or personal relationships that could have appeared to influence the work reported in this paper.

Acknowledgments

This work was jointly funded by the National Natural Science Foundation of China (Grant 42475129 and U2442205), and Xizang Science and Technology Innovation Base's Financial Support (Grant XZ202401YD0008).

Appendix A. Supplementary data

Supplementary data to this article can be found online at https://doi.org/10.1016/j.atmosres.2026.108898.

Data availability

All the data are available in the main text.

References

Bretherton, C.S., Widmann, M., Dymnikov, V.P., Wallace, J.M., Bladé, I., 1999. The effective number of spatial degrees of freedom of a time-varying field. J. Clim. 12, 1990–2009. https://doi.org/10.1175/1520-0442(1999)012<1990:TENOSD>2.0.CO;2.

Cao, X., Wu, R., Xu, J., Feng, J., Zhang, X., Dai, Y., Liu, Y., 2021. Contribution of the intensity of intraseasonal oscillation to the interannual variation of tropical cyclogenesis over the western North Pacific. Environ. Res. Commun. 3, 031002. https://doi.org/10.1088/2515-7620/abed93.

Cheng, Y., Wang, L., Li, T., 2020. Causes of interdecadal increase in the intraseasonal rainfall variability over Southern China around the early 1990s. J. Clim. 33, 9481–9496. https://doi.org/10.1175/JCLI-D-20-0047.1.

Diamond, H.J., Renwick, J.A., 2015. The climatological relationship between tropical cyclones in the southwest pacific and the Madden–Julian Oscillation. Int. J. Climatol. 35, 676–686. https://doi.org/10.1002/joc.4012.

Duan, A., Liu, S., Zhao, Y., Gao, K., Hu, W., 2018. Atmospheric heat source/sink dataset over the Tibetan Plateau based on satellite and routine meteorological observations. Big Earth Data. 2, 179–189. https://doi.org/10.1080/20964471.2018.1514143.

Duchon, C.E., 1979. Lanczos filtering in one and two dimensions. J. Appl. Meteorol. Climatol. 18, 1016–1022. https://doi.org/10.1175/1520-0450(1979)018<1016:LFIOAT>2.0.CO;2.

Fujinami, H., Yasunari, T., 2009. The effects of Midlatitude waves over and around the Tibetan Plateau on Submonthly Variability of the East Asian Summer Monsoon. Mon. Weather Rev. 137, 2286–2304. https://doi.org/10.1175/2009MWR2826.1.

Han, Y., Jiang, D., Si, D., Ma, Y., Ma, W., 2024. Time-lagged effects of the spring atmospheric heat source over the Tibetan Plateau on summer precipitation in Northeast China during 1961–2020: role of soil moisture. Adv. Atmos. Sci. 41, 1527–1538. https://doi.org/10.1007/s00376-023-2363-8.

Hendon, H.H., Zhang, C., Glick, J.D., 1999. Interannual variation of the Madden–Julian oscillation during Austral Summer. J. Clim. 12, 2538–2550. https://doi.org/10.1175/1520-0442(1999)012<2538:IVOTMJ>2.0.CO;2.

Hsu, P.-C., Lee, J.-Y., Ha, K.-J., 2016. Influence of boreal summer intraseasonal oscillation on rainfall extremes in southern China. Int. J. Climatol. 36, 1403–1412. https://doi.org/10.1002/joc.4433.

Jeong, J.-H., Kim, B.-M., Ho, C.-H., Noh, Y.-H., 2008. Systematic variation in wintertime precipitation in East Asia by MJO-induced extratropical vertical motion. J. Clim. 21, 788–801. https://doi.org/10.1175/2007JCLI1801.1.

Jiang, X., Li, T., Wang, B., 2004. Structures and mechanisms of the Northward Propagating Boreal Summer Intraseasonal Oscillation. J. Clim. 17, 1022–1039. https://doi.org/10.1175/1520-0442(2004)017<1022:SAMOTN>2.0.CO;2.

Kajikawa, Y., Yasunari, T., 2005. Interannual variability of the 10–25- and 30–60-day variation over the South China Sea during boreal summer. Geophys. Res. Lett. 32. https://doi.org/10.1029/2004GL021836.

Kan, Z.-T., Zhao, L., Li, Q.-Q., Shen, X.-Y., Ding, Y.-H., Liu, Y.-J., 2025. Impact of the winter Southern Indian Ocean Dipole on the summer precipitation pattern of southern flood and northern drought in China. J. Trop. Meteorol. 31, 257–270. https://doi.org/10.3724/j.1006-8775.2025.019.

Karmakar, N., Misra, V., 2019. The relation of intraseasonal variations with local onset and demise of the Indian Summer monsoon. J. Geophys. Res. Atmos. 124, 2483–2506. https://doi.org/10.1029/2018JD029642.

Kobayashi, S., Ota, Y., Harada, Y., Ebita, A., Moriya, M., Onoda, H., Onogi, K., Kamahori, H., Kobayashi, C., Endo, H., Miyaoka, K., Takahashi, K., 2015. The JRA-55 reanalysis: general specifications and basic characteristics. J. Meteorol. Soc. Japan. Ser. 2 93, 5–48. https://doi.org/10.2151/jmsj.2015-001.

Li, J., Mao, J., 2018. The impact of interactions between tropical and midlatitude intraseasonal oscillations around the Tibetan Plateau on the 1998 Yangtze floods. Q. J. R. Meteorol. Soc. 144, 1123–1139. https://doi.org/10.1002/qj.3279.

Li, G., Lu, H., Huang, C., Fan, Y., Zhang, B., 2016. A climatology of the surface heat source on the Tibetan Plateau in summer and its impacts on the formation of the tibetan plateau vortex. Chin. J. Atmos. Sci. 40, 131–141. https://doi.org/10.3878/j.issn.1006-9895.1504.15125.

Li, X., Gollan, G., Greatbatch, R.J., Lu, R., 2019. Impact of the MJO on the interannual variation of the Pacific–Japan mode of the East Asian summer monsoon. Clim. Dyn. 52, 3489–3501. https://doi.org/10.1007/s00382-018-4328-7.

Liu, F., Li, T., Wang, H., Deng, L., Zhang, Y., 2016a. Modulation of boreal summer intraseasonal oscillations over the Western North Pacific by ENSO. J. Clim. 29, 7189–7201. https://doi.org/10.1175/JCLI-D-15-0831.1.

Liu, F., Zhou, L., Ling, J., Fu, X., Huang, G., 2016b. Relationship between SST anomalies and the intensity of intraseasonal variability. Theor. Appl. Climatol. 124, 847–854. https://doi.org/10.1007/s00704-015-1458-2.

Liu, B., Chen, G., Qin, H., 2024. Joint impacts of intraseasonal oscillation and diurnal cycle on East Asian summer monsoon rainfall. J. Clim. 37, 77–95. https://doi.org/10.1175/JCLI-D-23-0284.1.

Lu, M., Yang, S., Fan, H., Wang, J., 2023. Interdecadal instability of the interannual connection between southern Tibetan Plateau precipitation and Southeast Asian summer monsoon. Atmos. Res. 291, 106825. https://doi.org/10.1016/j.atmosres.2023.106825.

Luo, H., Wang, Z., Wu, H., Zeng, Z., Yu, W., 2023. Weakened relationship between the Tibetan Plateau heat source and the Western North Pacific anomalous anticyclone in recent summers. J. Clim. 36, 5027–5040. https://doi.org/10.1175/JCLI-D-22-0727.1.

Luo, H., Wang, Z., He, C., Chen, D., Yang, S., 2024. Future changes in south Asian summer monsoon circulation under global warming: role of the Tibetan Plateau latent heating. npj Clim. Atmos. Sci. 7, 103. https://doi.org/10.1038/s41612-024-00653-x.

Luo, H., Yu, H., Hu, Z., Zhou, J., Cheng, S., Ren, Y., Wu, H., Gong, Y., 2025. Impact of summer atmospheric heat source over the Tibetan Plateau on the interannual variability of precipitation in Northwest China. Clim. Dyn. 63, 421. https://doi.org/10.1007/s00382-025-07928-w.

Madden, R.A., Julian, P.R., 1971. Detection of a 40–50 Day oscillation in the zonal wind in the tropical Pacific. J. Atmos. Sci. 28, 702–708. https://doi.org/10.1175/1520-0469(1971)028<0702:DOADOI>2.0.CO;2.

Madden, R.A., Julian, P.R., 1972. Description of global-scale circulation cells in the tropics with a 40–50 day period. J. Atmos. Sci. 29, 1109–1123. https://doi.org/10.1175/1520-0469(1972)029<1109:DOGSCC>2.0.CO;2.

Mao, J., Sun, Z., Wu, G., 2010. 20–50-day oscillation of summer Yangtze rainfall in response to intraseasonal variations in the subtropical high over the western North Pacific and South China Sea. Clim. Dyn. 34, 747–761. https://doi.org/10.1007/s00382-009-0628-2.

Muhammad, F.R., Lubis, S.W., 2023. Impacts of the boreal summer intraseasonal oscillation on precipitation extremes in Indonesia. Int. J. Climatol. 43, 1576–1592. https://doi.org/10.1002/joc.7934.

Peng, Y., He, J., Cheng, L., Zhang, B., 2012. A study on the characteristics and effect of the low-frequency oscillation of the atmospheric heat source over the eastern Tibetan Plateau from 1981 to 2000 (in Chinese). J. Trop. Meteorol. 28, 330–338. https://doi.org/10.3969/j.issn.1004-4965.2012.03.005.

Qi, Y., Zhang, R., Li, T., Wen, M., 2009. Impacts of intraseasonal oscillation on the onset and interannual variation of the Indian summer monsoon. Chin. Sci. Bull. 54, 880–884. https://doi.org/10.1007/s11434-008-0441-z.

Qi, Y., Li, T., Zhang, R., Chen, Y., 2019. Interannual relationship between intensity of rainfall intraseasonal oscillation and summer-mean rainfall over Yangtze River Basin in eastern China. Clim. Dyn. 53, 3089–3108. https://doi.org/10.1007/s00382-019-04680-w.

Raghavendra, A., Zhou, L., Roundy, P.E., Jiang, Y., Milrad, S.M., Hua, W., Xia, G., 2020. The MJO'S impact on rainfall trends over the Congo rainforest. Clim. Dyn. 54, 2683–2695. https://doi.org/10.1007/s00382-020-05133-5.

Ren, R., Zhu, C., Cai, M., 2019. Linking quasi-biweekly variability of the South Asian high to atmospheric heating over Tibetan Plateau in summer. Clim. Dyn. 53, 3419–3429. https://doi.org/10.1007/s00382-019-04713-4.

Song, L., Wu, R., An, L., 2019. Different sources of 10- to 30-day Intraseasonal Variations of Autumn Snow over Western and Eastern Tibetan Plateau. Geophys. Res. Lett. 46, 9118–9125. https://doi.org/10.1029/2019GL083852.

Takaya, K., Nakamura, H., 2001. A formulation of a phase-independent wave-activity flux for stationary and Migratory Quasigeostrophic Eddies on a Zonally varying basic flow. J. Atmos. Sci. 58, 608–627. https://doi.org/10.1175/1520-0469(2001)058<0608:AFOAPI>2.0.CO;2.

Tian, J., Yang, S., Liu, Y., 2023. Interannual Variation of the Quasi-biweekly Oscillation Intensity of Diabatic heating over the Tibetan Plateau during Boreal Summer and its Relationship with Rainfall Anomaly over Eastern China. Chin. J. Atmos. Sci. 47, 327–342. https://doi.org/10.3878/j.issn.1006-9895.2108.21106.

Wang, L., Chen, L., 2016. Interannual variation of convectively-coupled equatorial waves and their association with environmental factors. Dyn. Atmos. Oceans 76, 116–126. https://doi.org/10.1016/j.dynatmoce.2016.10.004.

Wang, M., Duan, A., 2015. Quasi-Biweekly Oscillation over the Tibetan Plateau and its link with the Asian Summer Monsoon. J. Clim. 28, 4921–4940. https://doi.org/10.1175/JCLI-D-14-00658.1.

Wang, Y., Wu, R., 2020. Patterns and factors of interannual variations of boreal summer intraseasonal oscillation intensity over tropical western North Pacific. Clim. Dyn. 54, 2085–2099. https://doi.org/10.1007/s00382-019-05100-9.

Wang, Y., Chen, L., He, J., Zhang, B., 2009. Effect of summer heat source low-frequency oscillation over the Tibetan Plateau on precipitation in Eastern China (in Chinese). J. Appl. Meteorol. Sci. 20, 419–427. https://doi.org/10.3969/j.issn.1001-7313.2009.04.005.

Wang, M., Wang, J., Duan, A., Liu, Y., Zhou, S., 2018. Coupling of the Quasi-Biweekly Oscillation of the Tibetan Plateau Summer Monsoon with the Arctic Oscillation. Geophys. Res. Lett. 45, 7756–7764. https://doi.org/10.1029/2018GL077136.

Wang, B., Chen, G., Liu, F., 2019a. Diversity of the Madden-Julian Oscillation. Sci. Adv. 5, eaax0220. https://doi.org/10.1126/sciadv.aax0220.

Wang, M., Wang, J., Duan, A., Yang, J., Liu, Y., 2019b. Quasi-biweekly impact of the atmospheric heat source over the Tibetan Plateau on summer rainfall in Eastern China. Clim. Dyn. 53, 4489–4504. https://doi.org/10.1007/s00382-019-04798-x.

Wang, Y., Wu, R., Gu, Q., 2022a. Asymmetric changes in intraseasonal oscillation intensity over the tropical Western North Pacific in El Niño and La Niña developing summers. J. Clim. 35, 2617–2631. https://doi.org/10.1175/JCLI-D-21-0615.1.

Wang, Z., Yang, S., Luo, H., Li, J., 2022b. Drying tendency over the southern slope of the Tibetan Plateau in recent decades: role of a CGT-like atmospheric change. Clim. Dyn. 59, 2801–2813. https://doi.org/10.1007/s00382-022-06262-9.

Wen, M., Yang, S., Higgins, W., Zhang, R., 2011. Characteristics of the dominant modes of atmospheric quasi-biweekly oscillation over tropical–subtropical Americas. J. Clim. 24, 3956–3970. https://doi.org/10.1175/2011JCLI3916.1.

Wu, J., Gao, X., 2013. A gridded daily observation dataset over China region and comparison with the other datasets (in Chinese). Chin. J. Geophys. 56, 1102–1111. https://doi.org/10.6038/cjg20130406.

Wu, G., He, B., Duan, A., Liu, Y., Yu, W., 2017. Formation and variation of the atmospheric heat source over the Tibetan Plateau and its climate effects. Adv. Atmos. Sci. 34, 1169–1184. https://doi.org/10.1007/s00376-017-7014-5.

Yanai, M., 1961. A detailed analysis of typhoon formation. J. Meteorolog. Soc. Jpn. Ser. II. 39, 187–214. https://doi.org/10.2151/jmsj1923.39.4_187.

Yanai, M., Esbensen, S., Chu, J.-H., 1973. Determination of bulk properties of tropical cloud clusters from large-scale heat and moisture budgets. J. Atmos. Sci. 30, 611–627. https://doi.org/10.1175/1520-0469(1973)030<0611:DOBPOT>2.0.CO;2.

Yang, S., Li, T., 2016. Intraseasonal variability of air temperature over the mid-high latitude Eurasia in boreal winter. Clim. Dyn. 47, 2155–2175. https://doi.org/10.1007/s00382-015-2956-8.

Yang, S., Li, T., 2017. Causes of intraseasonal diabatic heating variability over and near the Tibetan Plateau in boreal summer. Clim. Dyn. 49, 2385–2406. https://doi.org/10.1007/s00382-016-3463-2.

Yang, R., Tao, Y., Cao, J., 2010. A mechanism for the interannual variation of the early summer East Asia-Pacific teleconnection wave train. Acta. Meteor. Sin. 24, 452–458.

Yang, X., Huang, P., Liu, Y., Chen, D., 2022. An interdecadal enhancement of the impact of ENSO on the Summer Northeast Asian circulation around 1999/2000 through the silk road pattern. J. Clim. 35, 7481–7497. https://doi.org/10.1175/JCLI-D-22-0195.1.

Yao, Y., Lin, H., Wu, Q., 2019. Linkage between interannual variation of the East Asian Intraseasonal Oscillation and Mei-Yu Onset. J. Clim. 32, 145–160. https://doi.org/10.1175/JCLI-D-17-0873.1.

Yuan, Y., Hsu, P.-C., Li, W., 2023. Characteristics and dynamics of two distinct quasi-biweekly oscillations in the Tibetan Plateau summer monsoon. Clim. Dyn. 61, 91–109. https://doi.org/10.1007/s00382-022-06575-9.

Zeng, Z., Sun, J., 2023. Interannual Variations in the Intraseasonal Variability of Spring Precipitation over Southern China and the possible Mechanisms. J. Clim. 36, 5319–5336. https://doi.org/10.1175/JCLI-D-22-0863.1.

Zhang, K., Li, J., Zhu, Z., Li, T., 2021. Implications from subseasonal prediction skills of the prolonged heavy snow event over Southern China in early 2008. Adv. Atmos. Sci. 38, 1873–1888. https://doi.org/10.1007/s00376-021-0402-x.

Zhang, P., Duan, A., Wang, X., 2023. Joint effect of the Indian Ocean Dipole and the Silk Road Pattern on Indian rainfall during summer to autumn transition. Atmos. Res. 283, 106589. https://doi.org/10.1016/j.atmosres.2022.106589.

Zheng, C., Chang, E.K.M., 2019. The role of MJO propagation, lifetime, and intensity on modulating the temporal evolution of the MJO extratropical response. J. Geophys. Res. Atmos. 124, 5352–5378. https://doi.org/10.1029/2019JD030258.

Zhong, S., Jia, Q., Zhu, Z., Zhang, X., 2020. Two propagation pathways of the boreal summer Quasi-Biweekly oscillation of the atmospheric heat source over the Tibetan Plateau. Atmosphere-Ocean 58, 60–78. https://doi.org/10.1080/07055900.2020.1730297.

Zhu, C., Ren, R., Wu, G., 2018. Varying Rossby wave trains from the developing to decaying period of the upper atmospheric heat source over the Tibetan Plateau in boreal summer. Adv. Atmos. Sci. 35, 1114–1128. https://doi.org/10.1007/s00376-017-7231-y.

Zhu, Z., Feng, Y., Jiang, W., Lu, R., Yang, Y., 2023. The compound impacts of sea surface temperature modes in the Indian and North Atlantic oceans on the extreme precipitation days in the Yangtze River Basin. Clim. Dyn. 61, 3327–3341. https://doi.org/10.1007/s00382-023-06733-7.

Zhu, Z., Wang, M., Wang, J., Duan, A., Liu, B., Yu, Z., 2025. Intraseasonal oscillation intensity variations of the atmospheric heat source over the Tibetan Plateau and their relationship with summer precipitation. J. Clim. 38, 931–946. https://doi.org/10.1175/JCLI-D-24-0216.1.